PAPER

Experimental search for low energy nuclear excitation by femtosecond plasma

IOP Publishing | Astro Ltd Laser Physics
Laser Phys. **24** (2014) 116002 (7pp) doi:10.1088/1054-660X/24/11/116002

Experimental search for low energy nuclear excitation by femtosecond plasma

O V Chefonov[1], A V Ovchinnikov[1], A A Yurkevich[1], S A Romashevskiy[1], S A Shulyapov[2], V P Petrovskiy[1], A B Savel'ev[1,2] and M B Agranat[1]

[1] Joint Institute for High Temperatures of Russian Academy of Sciences, Izhorskaya st. 13, Bd. 2, Moscow 125412, Russia
[2] Physics Faculty and International Laser Center of M V Lomonosov Moscow State University, Leninskie gory, Moscow 119991, Russia

E-mail: a.ovtch@gmail.com

Received 27 June 2014, revised 13 August 2014
Accepted for publication 18 August 2014
Published 2 October 2014

Abstract

New experimental data on the secondary electron yield from a thin layer of ^{57}Fe irradiated by emission of the hot dense plasma source created by femtosecond laser pulses with intensity of 10^{17} W cm^{-2} is presented. Plasma source hard x-ray and electron fluxes are measured for the source characterization. Thorough statistical analysis of the delayed secondary electron spectrum from the ^{57}Fe layer in the 20–100 ns temporal window allows exclusion of the 'null' hypothesis of the random character of the differences of this spectrum with that obtained using a ^{56}Fe target. Thus, statistically valid maxima at ~5.8 and 7.4 keV can be attributed to the decay of the isomeric nuclear state of ^{57}Fe (3/2$^-$, 14.41 keV, 98 ns) by the internal conversion process through the atomic *K*-shell (maximum at 7.4 keV), followed by the Auger process (maximum at 5.8 keV).

Keywords: femtosecond laser plasma, x-ray, electrons, isomeric nuclear state, excitation, isotope, internal conversion

(Some figures may appear in colour only in the online journal)

1. Introduction

The excitation of low energy isomeric states in laser-produced plasma has been intensively studied over a long time (see [1, 2] and references therein). However, conclusive experimental data that could confirm the possibility of such processes are still lacking. Previous works with encouraging results [2, 3] have been questioned by other experimental data [4] and theoretical calculations [5]. Although the feasibility of such processes is obvious, detection of a single event of excited isomeric state decay over the 'noise' due to intense particle and electromagnetic plasma emission is the main experimental difficulty [6, 7, 9].

A novel approach using two sets of targets and time-delayed detection of emitted radiation was applied in recent works [8, 9] to overcome the above mentioned difficulties. Emission of plasma produced at a primary target under femtosecond laser irradiation was used as an excitation source for the isomeric state of the ^{57}Fe isotope layer on top of a secondary target placed 20 cm from the first [9]. In this case, the semi-cylindrical electrostatic analyzer can be placed quite close to the secondary target, and enhancement in the solid angle of the detector compensates for a drop in the fluence of exciting radiation. In [9], due to the low repetition rate of laser pulses (10 Hz), the signal-to-noise ratio was not high enough to make statistically significant conclusions as to whether the observed electrons were from internal electronic conversion.

In this work, we attempted to obtain more reliable data with a 1 kHz femtosecond laser following the basic scheme described in [9]. We began with the experimental study of plasma emission and measured the x-ray and electron fluxes from plasma. Results are presented in section 3. The detection of single delayed electrons from the secondary target is described in section 4. Finally, we made thorough statistical verification of the data and showed that our data supports the existence of spectral peaks at energies corresponding to the 3/2$^-$ (14.41 keV, 98 ns) isomeric level of ^{57}Fe nuclei decay via internal electronic conversion (IEC).

2. Experimental setup and measurements

In our scheme, the interaction of intense femtosecond laser pulses with a solid-state target led to generation of hot dense laser plasma. Irradiation of the secondary target, containing ^{57}Fe nuclei in the ground state (1/2$^-$, 0.0), by x-ray and particle radiation from the primary target resulted in excitation and the subsequent decay of the first excited state 3/2$^-$ (14.41 keV, 98 ns) of ^{57}Fe nuclei by the IEC process. In the experiment, the presence of two space-separated targets and use of a time-resolved semi-cylindrical electrostatic analyzer made it possible to resolve time events of nuclear decay from the hot laser plasma emission. However, extremely low efficiency of the nuclei excitation process due to a low excitation cross-section, a strong resonant photoabsorption, and an extremely narrow linewidth of nuclear ground-isomeric state transition [10] impose restrictions on laser-plasma source characteristics of exciting radiation, particularly on spectral-angular distribution of radiation flux density. On the other hand, a high radiation background from a laser-plasma source requires necessary measures to be taken for signal enhancement and noise suppression within the experimental procedures.

Our experiments were carried out with the Ti:sapphire laser system based on chirped pulse amplification and consisting of a femtosecond laser oscillator, stretcher, regenerative amplifier, and compressor. This laser system is a part of the unique scientific facility 'Terawatt Femtosecond Laser Complex' at the Joint Institute for High Temperatures of the Russian Academy of Sciences. The laser operates at a 1 kHz repetition rate at the central wavelength of 795 nm. The pulse duration, measured with a second-order autocorrelator, was 40 fs FWHM. The maximum laser energy on the target was 1.5 mJ. The laser pulse contrast ratio over a nanosecond temporal range (controlled by electro-optical shutter) was $\sim 10^{-8}$ and over a picosecond temporal range was 10^{-5}.

The laser beam was focused on the first target using a two-inch off-axis parabola with effective focal distance of 76.2 mm and reflectivity of 97% . The spatial distribution of the focused laser beam on the first target was measured by the CCD-based imaging system and its cross-section was fitted with a Gaussian function, shown in figure 1 by a dashed line. According to the measured data, the diameter of the laser beam was 5.5 μm at FWe^{-1}M and the laser beam incidence angle was 45° (p-polarized). The estimation of the incident laser intensity (on the assumption that the focal spot contains ~70% of laser pulse energy) was $I \sim 10^{17}$ W cm^{-2}.

The target was fixed to an optical holder and mounted to the motorized three-axes vacuum translator. The translator controller has an option of synchronizing the start of the x-axis translator with the Pockels cell of the regenerative amplifier. Thus, the laser works only if the translator is in operation.

The size of the laser focal spot on the target plane was monitored with an imaging system coupled to a CCD detector. A 20 μm thick Mylar film shielded the parabolic mirror from the debris produced by the interaction of laser pulses with the target. To refresh the film during the experiment, it was mounted to a tape-moving device.

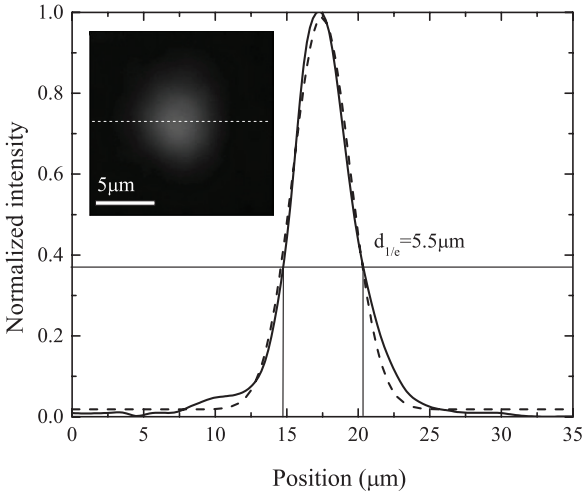

Figure 1. Cross-section of the spatial distribution of laser intensity (shown in the inset) at the focal spot on the target.

The interaction of laser radiation with the target took place in a vacuum chamber evacuated to 10^{-5} Torr by an oil-free turbomolecular pump (Varian Turbo-V 550). A plane-parallel plate made of tungsten 25 × 25 mm^{2}in size and 2 mm thick was used as a first target.

X-ray radiation diagnostics were realized with an assembly of several 25 mm thick NaI(Tl) scintillators coupled to FEU-91 photomultipliers and an Amptek XR-100T-Cd x-ray spectrometer (CdTe crystal with digital processor PX-4). A semi-cylindrical electrostatic analyzer composed of a semi-cylindrical capacitor and a shevron multichannel plate detector VEU-7 was used for detection of the laser plasma particle radiation and IEC electrons. Signals from the scintillation detectors and VEU-7 were recorded by means of a Tektronix TDS7054 storage oscilloscope. The experimental setup is shown in figure 2.

3. Plasma characterization

To specify characteristics of the laser-plasma source and associated excited radiation, the electron and x-ray energy distributions were measured and the hot electron temperature was estimated. To measure the spectral distribution of x-ray radiation the Amptek XR-100T-Cd spectrometer was placed 12 cm away from the flange of the vacuum chamber, looking at the target through a 6 μm-thick mylar window. The total distance from the radiation source to the spectrometer was 90 cm. To provide the required radiation load for the spectrometer, a collimator with 400 μm-diameter aperture was set up in front of the detector. The average time of x-ray spectrum accumulation did not exceed 30 s, which is equivalent to 30 000 laser shots. To provide a qualitative assessment of the x-ray radiation pattern, x-ray spectra were measured for two observation angles: along the target normal and in the direction of the specular reflection of the laser pulse. According to the measured data, there was an angular anisotropy in the x-ray yield: the x-ray yield along the target normal was two times higher than the yield in the specular direction. This is in good agreement with

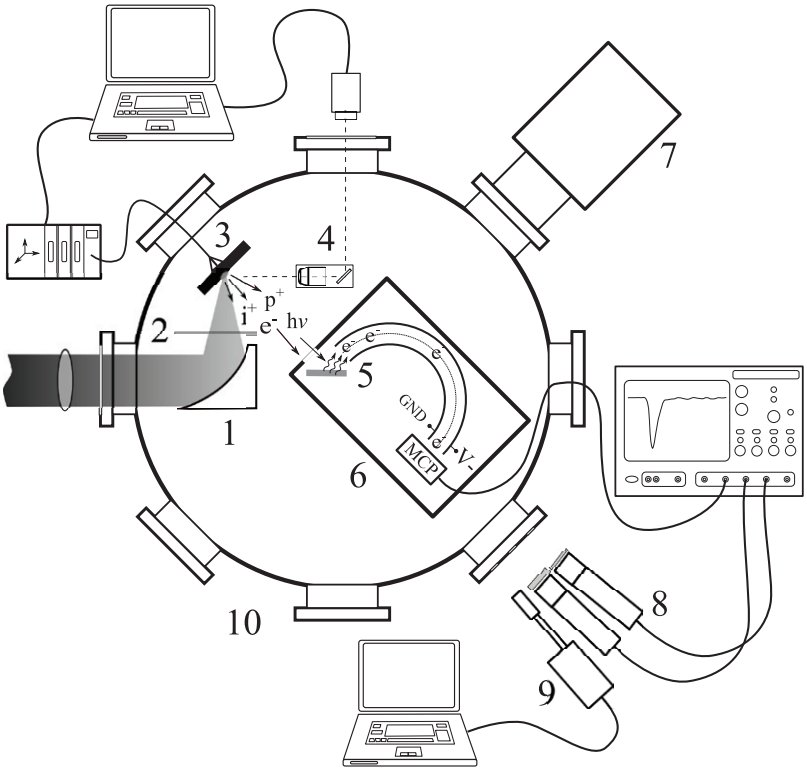

Figure 2. The experimental setup: 1—off-axis parabolic mirror, 2—protective Mylar film, 3—primary target, 4—imaging system coupled to a CCD detector, 5—secondary target, 6—electrostatic spectrometer, 7—vacuum pump, 8—scintillator detectors, 9—spectrometer Amptek XR-100T-Cd, 10—vacuum chamber.

the well-known $\cos^2\phi$ dependence [11], where ϕ is the angle between the target normal and the observation direction. The spectral density of x-ray photon flux along the target normal is shown in the figure 3, taking into account x-ray attenuation in the energy window, solid angle, and spectrometer efficiency. Two components are clearly visible—line radiation to the L atomic shell around 8–10 keV and smooth background due to bremsstrahlung emission.

The measured spectral distribution of direct electron flux from plasma in 5–30 keV energy range for two angles of emission of 0 and 45 degrees is presented in figure 4. The secondary target was removed and the spectrometer input slit looked directly at the laser plasma source for this measurement. The semi-cylindrical capacitor, multichannel plate frame, and high-voltage divider were placed in the special shielding case with an outer lead screen to reduce electromagnetic interference and noise from low energy x-ray photons and electrons impacting directly on the analyzer cables and other parts of the detecting system. All the signal cables connecting the analyzer with the oscilloscope and high-voltage power supplies were protected with outer grounded electrostatic screens to improve noise immunity of the entire system. The spectral energy distribution of electrons was measured by the sequential change of the deflection biasing of the capacitor plates. The energy resolution of the spectrometer was determined by its configuration and amounted to 10%, while maximum energy of a detected particle per its charge (∼ 35 keV per unit charge) was determined by the highest possible voltage biased to the capacitor and was limited by electric breakdown inside the spectrometer.

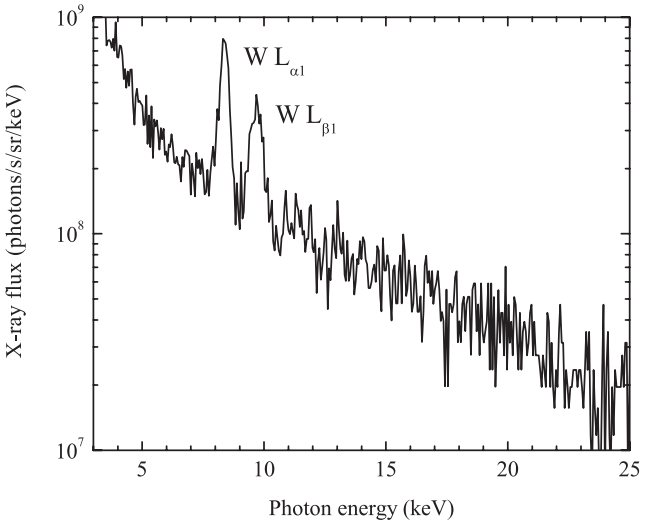

Figure 3. Spectral density of x-ray photon flux along the primary target normal from the femtosecond laser plasma at intensity of $\sim 10^{17}$ W cm^{-2}. (The primary target was tungsten and the data were collected without time-delay.)

The spectrometer was placed 25 cm from the primary target, and solid detection angle was determined by the 2 mm-diameter aperture mounted on the entrance window of the shielding case of the spectrometer. We accumulated ∼16 000 laser shots for each energy channel of the spectrum.

The values in figure 4 correspond to the flux of electrons with a given energy E for a single laser shot in a unit solid

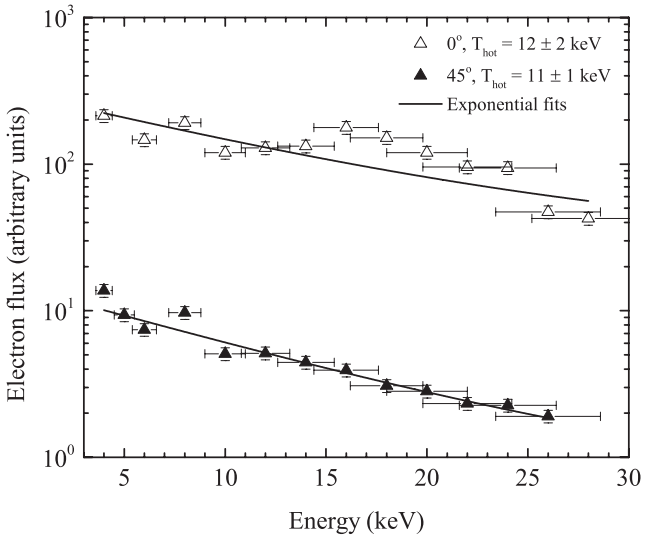

Figure 4. Measured spectral distribution of accelerated electrons from femtosecond laser plasma at intensity of ~10^{17} W cm^{-2} along the target normal (open triangles) and along the specular direction (solid triangles). Solid lines present the exponential fits that determined the hot electron temperature T_{hot}. (The primary target was tungsten, and the data were collected without time-delay.)

angle and in the same energy range ΔE. We assumed here that the gain factor of the VEU-7 detector is not dependent on the detected electron energy E. The latter factor is the product of detection efficiency and a gain factor of the multichannel plate (MCP) assembly (output-to-input current ratio of the MCP) that, in turn, depends on the MCP biasing, secondary electrons emission rate, and the MCP detector design. Hence, we do not insert absolute values along the ordinate axis in figure 4.

According to the measured data, electrons are accelerated predominantly along the target normal: a 20-fold increase in the electron yield is clearly visible in figure 4. In case of a 3D Maxwellian distribution of hot electron energy with temperature T_{hot}, the distribution reads as

$$f_e(E) \sim \exp\left(-\frac{E}{T_{hot}}\right). \quad (1)$$

The x-ray emission power spectral density can be written as [11]:

$$G(E, T_{hot}) \propto \frac{1}{\sqrt{T_{hot}}} \exp\left(-\frac{h\nu}{T_{hot}}\right), \quad (2)$$

so the hot electron temperature T_{hot} can be estimated both directly from energy distribution of electrons and indirectly from the x-ray spectrum by approximating the measured data with functions (1) (fitting lines in figure 4) and (2), respectively. The exponential fits in figure 4 provide nearly the same values for the hot electron temperature: $T_{hot} = 12 \pm 2$ keV at $\phi = 0°$ and $T_{hot} = 11 \pm 1$ keV at $\phi = 45°$.

The fit of the high energy tail in figure 3 (above 25 keV) yielded $T_{hot} = 8 \pm 2$ keV. Integrated hard x-ray measurements taken with the PMT based scintillator detectors (x-rays above 30 keV) using the filter method [11, 12] showed that the corresponding hot electron temperature was somewhat higher—$T_{hot} = 17 \pm 2$ keV. The total number of hot electrons generated in one laser shot can be estimated as the ratio of laser pulse energy E_{las} to the average energy of hot electrons $\langle E_{hot} \rangle = \frac{3}{2} T_{hot}$ multiplied by the conversion efficiency η of laser energy to hot electron energy. For example, for $E_{las} = 1$ mJ, $\langle E_{hot} \rangle = 18$ keV, and $\eta \sim 1\%$ [10] the total number of hot electrons is 3×10^9.

Hence, the laser-plasma source, created on the surface of a tungsten solid target by femtosecond laser pulses at intensity of ~10^{17} W cm^{-2} and 1 kHz repetition rate possesses the necessary spectral components for excitation of low-lying isomeric state $3/2^-$ (14.41 keV, 98 ns) of ^{57}Fe nuclei.

4. Registration of delayed electrons from the secondary target

A silicon substrate (400 μm–thick with area 1×1 cm^2) coated with a 100 nm thick layer of iron enriched with ^{57}Fe isotope up to 98% was used as the secondary target (see figure 1). It was mounted directly in front of the entrance slit (with aperture 3×1 cm^2) of the semi-cylindrical capacitor, 2 cm from the slit and inside the shielded case of the electrostatic analyzer. The target was tilted by 45° both in the direction to the primary target and to the center of the slit. The radiation from the laser-plasma source irradiated the secondary target through the aperture (8 mm in diameter) set up on the side wall of the shielding case. This aperture looked at the primary target in the direction tilted by 45° to the target normal. The distance from the plasma source to the aperture was 22 cm, and the distance from the aperture to the secondary target was 3 cm.

In our experiments, we aimed to detect the following process. The low-lying isomeric state of ^{57}Fe nucleus with energy of 14.41 keV and lifetime of 98 ns undergoes excitation under exposure of the secondary target to plasma radiation. IEC of an excited nucleus competes with gamma-decay and occurs if the energy of the nuclear transition exceeds the binding energy of an electron in an atomic shell [9]. In this case, non-radiative transfer of energy from an excited nucleus to a valence electron occurs and the latter leaves the atom. Hence, the energy of an ejected electron is equal to the difference between the energy of the isomeric nuclear state and the binding energy of the valence electron. To characterize this decay process, the internal conversion coefficient α is commonly used, which is the ratio of probabilities of the IEC and gamma decay channels. The internal conversion coefficient α is equal to 8.56 for the 14.41 keV isomeric state of the ^{57}Fe nucleus. According to the calculations [9, 14], the IEC process from the K-shell of an Fe atom (binding energy 7.113 keV) is the most probable decay process. An ejected electron will have kinetic energy of ~7.3 keV and the generated vacancy in the shell is filled by an electron from an outer shell. The latter process activates an Auger cascade, resulting in characteristic x-ray emission and/or Auger electron ejection. If the vacancy appears in the K-shell of an Fe atom, Auger *KLL*-transition is the most probable process, yielding electrons in the 5.5–5.7 keV energy range [9].

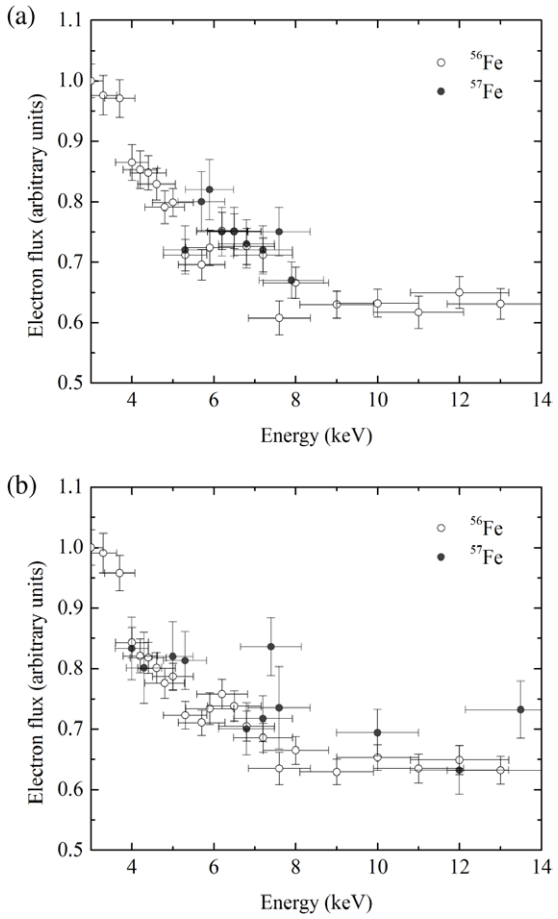

Figure 5. Normalized energy distributions of mean value of the number of electrons for ^{56}Fe (dataset 3, open circles) and ^{57}Fe (solid circles) for datasets 1 (*a*) and 2 (*b*).

Therefore, one can expect to observe (during the isomeric state lifetime) delayed electrons with energies corresponding to the IEC process through the *K*-shell (energy ∼ 7.3 keV) and Auger electrons (energy ∼ 5.6 keV) as well as background electrons caused by ionization of bound electrons by plasma accelerated ions [15]. Comparing data recorded with ^{57}Fe and ^{56}Fe samples (in the latter case the lowest nuclear state is 2^+, 846.78 keV, 6.07 ps, which was scarcely exited in our experimental conditions), one can distinguish if nuclear excitation occurs: ^{56}Fe and ^{57}Fe isotopes have the same atomic shell structure and binding energies so the only cause of changes in spectra should be linked to the appearance of IEC electrons from the 14.41 keV level decay.

The experimental results are shown in figure 5. The monitored energy range of electrons was 3–14 keV, with accumulation of 111 000 measurements for each energy (one measurement corresponds to one laser shot) in the experiment with the ^{56}Fe sample (dataset 3). In the case of the ^{57}Fe sample, two series were conducted in the energy range of 5–11 keV (dataset 1) and 4–13.5 keV (dataset 2). The number of measurements for each energy value was 41 000. To build the energy distribution, we chose the time interval from 20 ns to 100 ns after irradiation of the secondary target for further analysis. The lower limit relates to the termination of the huge signal from scattered electrons and x-rays originating from plasma. The upper limit is restrained by the lifetime of the ^{57}Fe nucleus isomeric state (98 ns). Each measurement was analyzed in this interval by searching for single electron detection events—short spikes with amplitudes above 20 mV and well above the noise level (∼ 1 mV). The spectra presented in figure 5 are the result of the summation of all such events for a given electron energy (determined by the analyzer voltage). Horizontal error bars in figure 5 reflect analyzer resolution, while vertical bars are statistical errors, discussed in the next section.

5. Statistical analysis

For statistical analysis of datasets, the following procedure was used. All three experimental datasets obtained were divided into consequential groups, each containing one thousand measurements. For each group, zero measurements were excluded. The mean value $N_j(E)$ of the number of registered electrons in a group j was calculated for each dataset and for each energy E. Thus, random quota samples—'the number of registered electrons with the same energy'—were obtained for each dataset. Overall, there were 26 samples in dataset 3, 14 samples in dataset 1, and 12 samples in dataset 2. Next, mean values $N_0(E)$ and standard deviations $S(E)$ were calculated for all the samples and only groups with mean value $N_j(E)$, satisfying the relationship $N_0(E) - 2S(E) \leqslant N_j(E) \leqslant N_0(E) + 2S(E)$, were used for further analysis. Thus, for each value E, sizes of samples were reduced to 35–39 for datasets 1 and 2 and 97–111 for dataset 3.

For the next step, the mean value $N_0(E)$ and standard deviation $S(E)$ were re-calculated for each sample. Then, the Pearson criterion was applied to check the normalcy of random variable's distribution for each sample. It was determined that the values of criterion measure χ_i^2, $i = 1, 26$, with degrees of freedom $\upsilon = 19$ are in the 4.2–21.5 range, while P-values are greater than 25% . Hence, the 'null' hypothesis concerning the normalcy of random variable distributions is fulfilled. The normalized ensemble of mean values $N_0(E_i)$, $i = 1, 26$ of the number of electrons with energy E_i in the ^{56}Fe case was used as the reference ensemble of mean values for measurements with ^{57}Fe.

Normalization of ensemble $\left\{N_0^{(1)}(E_i), S_0^{(1)}(E_i), i = 1..14\right\}$ for dataset 1 was performed, demanding the sum of squared deviations of $N_0^{(1)}(E_i)$ from $N_0(E_i)$ for energies $E_i \in$ (5.3 keV, 6.2 keV, 6.5 keV, 6.8 keV, 7.9 keV) reached the minimum value. A similar procedure for ensemble $\left\{N_0^{(2)}(E_i), S_0^{(2)}(E_i), i = 1..12\right\}$ for dataset 2 was carried out with $E_i \in$ (4.0 keV, 4.3 keV, 6.8 keV, 7.9 keV, 12.0 keV).

Figure 5 presents the normalized values of the mean number of electrons for datasets 1 and 2 obtained following the above described procedure along with reference values from dataset 3.

The assumption that for each E_i sample $\{N_j(E_i), j = 1..n_i\}$ of dataset 3 and $\left\{N_j^{(1)}(E_i), j = 1..m_i\right\}$ of dataset 1 $\left(\left\{N_j^{(2)}(E_i), j = 1..k_i\right\}$—for dataset 2) belong to the same parent population, i.e. differences between $N_0(E_i)$ and $N_0^{(1)}(E_i)$

Table 1. 'Null' hypothesis statistics

Energy, keV	υ	t	P-val, %	p, %
dataset 1				
5.3	73	0.1	90	10
5.7	57	2.0	5	95
5.9	61	1.7	9	91
6.2	69	1.1	41	59
6.8	79	0.4	71	29
7.2	77	0.5	65	35
7.6	71	2.8	1	99
7.9	79	0.1	88	12
dataset 2				
5.0	46	0.5	60	40
5.3	54	1.7	10	90
6.8	60	0.1	92	8
7.2	68	0.7	49	51
7.4	63	2.1	5	95
7.6	50	1.4	18	82
10	59	0.9	35	65
12	65	0.4	72	28
13.5	58	1.1	29	71

Table 1 shows for each value of energy E: (1) degrees of freedom number υ for the t-distribution, (2) t-statistics, (3) the P-value, which characterizes the probability of wrongly rejecting the 'null' hypothesis, and (4) p—the probability of rejecting the 'null' hypothesis. Calculations show that for dataset 1 at E_i = (5.7 keV, 5.9 keV, 7.6 keV), the 'null' hypothesis is rejected with event rates 95%, 91%, and 99%, respectively. For dataset 2, statistically significant differences are reached at E_i = (5.3 keV, 7.4 keV) with event rate 90%, 95%, respectively.

$(N_0^{(2)}(E_i))$ have random character, was used as the 'null' hypothesis. The Student criterion for independent samples was used to check this hypothesis. We calculated (i) degrees of freedom number υ for the t-distribution, (ii) the t-statistics, and (iii) the P-value characterizing the probability to reject the 'null' hypothesis wrongly.

Table 1 summarizes the statistical data treatment. It is evident that the 'null' hypothesis can be rejected for delayed electron energies of 5.7–5.9 keV and 7.4–7.6 keV (marked in grey), i.e. in the vicinity of energies corresponding to IEC decay of the 14.41 keV isomeric level of the ^{57}Fe nucleus and the subsequent Auger decay process.

6. Conclusion

We utilized the double target scheme for the study of low energy nuclear excitation. Here, the first target was used to form a high intensity flux of x-rays and electrons from plasma created by a super intense femtosecond laser pulse, while the secondary target contained the nuclei under study (as a sputtered thin layer). Such a scheme does not consume a nuclear isotope and greatly enhances the signal-to-noise ratio. Experiments were conducted with the ^{57}Fe isotope with a 14.41 keV isomeric nuclear state (with electronic conversion coefficient of 8.5 ns and 98 ns lifetime) and with the ^{56}Fe isotope (with the lowest nuclear level of 846.78 keV). Measurements of the secondary electron yield and spectra by semi-cylindrical electron analyzer showed that the spectrum from the ^{57}Fe sample obtained within a 20–100 ns temporal window contains maxima at ~5.8 and 7.4 keV that can be attributed to the isomeric 14.41 keV level de-excited by the internal conversion process through the atomic K-shell (maximum at 7.4 keV), followed by the Auger process (maximum at 5.8 keV). The spectrum observed for the ^{56}Fe sample does not exhibit any maxima. The thorough statistical analysis allows the conclusion that the difference between secondary electron yields for the two samples is statistically meaningful.

Our data show the same secondary electron yield from the second target as in the previous study [9], where the data were obtained with poorer statistics and larger systematic bias due to the lower repetition rate of the laser (10 Hz in [9] as compared to 1 kHz in our work) and slower data acquisition. Consequently, as in [9], the estimated excited nuclei yield was much higher in our experiment than the calculated yield. The high accuracy statistical analysis presented in our paper shows that either one is needed to find another explanation for the observed maxima (from some exotic process in the atomic core), or that the isomeric level excitation in our experiment is not well described by the existing theories.

Acknowledgments

These experimental investigations were carried out using the unique scientific facility 'Terawatt Femtosecond Laser Complex' at the Joint Institute for High Temperatures of the Russian Academy of Sciences www.ckp-rf.ru/usu/73613/.

References

[1] Andreev A V, Gordienko V M and Savel'ev A B 2001 Nuclear processes in a high-temperature plasma produced by an ultrashort laser pulse *Quantum Electron.* **31** 941–56
[2] Andreev A V *et al* 1999 Excitation of tantalum-181 nuclei in a high-temperature femtosecond laser plasma *J. Exp. Theor. Phys. Lett.* **69** 371–6
[3] Andreev A V *et al* 2000 Excitation and decay of low-lying nuclear states in a dense plasma produced by a subpicosecond laser pulse *J. Exp. Theor. Phys.* **91** 1163–75
[4] Gobet F *et al* 2008 Particle characterization for the evaluation of the 181mTa excitation yield in millijoule laser induced plasmas *J. Phys. B: At. Mol. Opt. Phys.* **41** 145701
[5] Gobet F *et al* 2011 Nuclear physics studies using high energy lasers *Nucl. Instrum. Methods Phys. Res.* A **653** 80–3
[6] Afonin V, Kakshin A and MazuninA 2010 Experimental study of the excitation of rhodium isomer in a plasma produced by a picosecond laser pulse *Plasma Phys. Rep.* **36** 250–5
[7] Afonin V, Vikhlyaev D, Kakshin A and Mazunin A 2011 Excitation of the isomeric states of silver isotope nuclei in the plasma produced by a subrelativistic picosecond laser pulse *Plasma Phys. Rep.* **37** 615–20
[8] Andreev A A *et al* 2002 Determination of the radiation cross sections of low-energy transitions of isomeric nuclei from observation of laser-induced γ fluorescence *J. Exp. Theor. Phys.* **94** 862–8
[9] Golovin G V, Savel'ev A B, Uryupina D S and Volkov R V 2011 Internal electron conversion of the isomeric ^{57} Fe nucleus state with an energy of 14.4 keV excited by the radiation of the plasma of a high-power femtosecond laser pulse *Quantum Electron.* **41** 222–6

[10] Tkalya E V 2004 Mechanisms for the excitation of atomic nuclei in hot dense plasma *Laser Phys.* **14** 360–77
[11] Giulietti D and Gizzi L A 1998 X-ray emission from laser produced plasmas *Riv. Nuovo Cimento* **21** 1
[12] Gordienko V M *et al* 2002 Experimental characterization of hot electron production under femtosecond laser plasma interaction at moderate intensities *Plasma Phys. Contol. Fusion* **44** 2555–68
[13] Kostenko O F, Ovchinnokov A V, Chefonov O V, Romashevskiy S A, Petrovskiy V P, Reev N E and Agranat M B 2014 Investigation of characteristic x-rays and hot-electron temperature in the interaction of normally incident femtosecond laser pulses with nanostructured foils *Phys. Scr.* **89** 075605
[14] Kibedi T, Burrows T W, Trzhaskovskaya M B, Davidson P M and Nestor C W Jr 2008 Evaluation of theoretical conversion coefficients using BrIcc *Nucl. Instrum. Methods* A **589** 202–29
[15] Golovin G V, Savel'ev A B, Uryupina D S, Volkov R V and Marin B V 2009 Observation of high energy electrons from a metal target irradiated by protons with a mean energy of 25 keV *JETP Lett.* **89** 492–5